*Friction* **8**(3): 604–612 (2020)
https://doi.org/10.1007/s40544-019-0307-1
ISSN 2223-7690
CN 10-1237/TH
RESEARCH ARTICLE

# Morphology and electric potential-induced mechanical behavior of metallic porous nanostructures

**Sunghan KIM**[1,*], **Andreas A. POLYCARPOU**[2], **Hong LIANG**[2,*]

[1] *School of Mechanical Engineering, Chung-Ang University, Seoul 06974, Republic of Korea*

[2] *Department of Mechanical Engineering, Texas A&M University, College Station 77843-3123, USA*

*Received: 11 April 2019 / Revised: 04 May 2019 / Accepted: 30 May 2019*



**Abstract:** Understanding mechanical behaviors influenced by electric potential and tribological contacts is important for verifying the robustness and reliability of applications based on metallic porous nanostructures in electrical stimulations. In this work, nickel-based metallic porous nanostructures were studied to characterize their mechanical properties and morphologically dependent contact areas during application of an electric potential using a nanoindenter. We observed that the indentation moduli of nickel-based metallic porous nanostructures were altered by pore size and application of electric potential. In addition, the structural aspects of the surface morphology of nickel-based porous nanostructures had a critical effect on the determination of contact area. We suggest that the relation between electric potential and the mechanical behaviors of metallic porous nanostructures can be crucial for building mechanically robust functional devices, which are influenced by electric potential. The morphological shape characteristics of metallic porous nanostructures can be alternative decisive factors for manipulation of tribological performance through regulation of contact area.

**Keywords:** mechanical properties; nanoindentation; metallic porous nanostructures; contact area; electric potentia

## 1 Introduction

Metallic nanostructures have many desirable and superior capabilities that have been widely studied to extend their scientific utilization and the versatility of their engineering applications. For example, noble metal nanostructures, such as copper, silver, and gold, are employed to convert solar energy to chemical energy [1]. Complex metallic nanostructures have been engineered to manipulate surface-enhanced Raman scattering (SERS) substrates for bio-sensors [2, 3]. Tin oxide nanostructures with copper deposits exhibited excellent hydrogen sulfide detection performance [4]. Nanostructural films comprised of implantable and biocompatible metals, such as titanium and tantalum, are used in artificial orthopedic and dental implants to enhance resistance to wear in order to improve durability [5]. Recently, nanostructural metal surfaces and nanopatterned, textile-based metal structures have attracted interest for fabrication of effective triboelectric nanogenerators (TENGs) [6–8]. Among popular metallic nanostructures, metallic porous nanostructures possess outstanding functional properties. They are of particular interest for the design of robust biomedical devices, flexible electronic devices, and energy harvesting/storage systems [9–12].

Metallic porous nanostructures exhibit excellent mechanical properties, superior tribological performance, large surface areas, good electrical conductivity, and potential catalytic capability [13–21]. Nickel-based metallic porous nanostructures, which form a subset of metallic porous nanostructures, possess desirable and unique properties owing to their exceptional structural stability and facile surface modification

* Corresponding authors: Sunghan KIM, E-mail: sunghankim@cau.ac.kr; Hong LIANG, E-mail: hliang@tamu.edu

[22, 23]. Three-dimensional (3D) porous nickel nanostructures have been used in the fabrication of highly sensitive glucose detection devices that do not employ enzymes [24]. A porous nickel-based TENG system has been devised for harvesting mechanical energy, which is then used to supply electric power for portable electronics [25]. Porous nickel-based superhierarchical nanocomposite electrodes used as anodes for lithium-ion batteries enhanced their electrochemical performance [26]. For the design of durable porous nickel-based micro/nanosystems, the mechanical properties of nickel porous nanostructures must be characterized, and a detailed understanding of their 3D structural features is needed. However, morphological and structural influences on the mechanical properties of nickel porous nanostructures have not been thoroughly studied.

In the present study, we explored the mechanical behavior of nickel-based, well-ordered metallic porous nanostructures by performing a nanoindentation experiment with a nanoindenter. Understanding the mechanical properties of metallic nanostructures induced by applied electric potential is critical for the design of robust, functional structural devices that operate under the influence of electric potential [27–29]. By applying an electric potential, we were able to investigate the indentation moduli of nickel-based, well-ordered porous nanostructures to determine the influence of electric voltage on the mechanical behavior of the nanostructures. We found that indentation moduli of the nanostructures were altered by pore size and application of electric potential. In addition, the contact area between the nanostructure surfaces and the indenter tip were systematically determined by in-depth morphological analysis of the nanostructures. We confirmed that detailed features of the surface morphologies of nickel porous nanostructures are crucial for determining the contact area. Understanding contact area in the context of the present work is critically important for future studies that focus on the durability and reliability of diverse scientific applications based on metallic porous nanostructures.

## 2 Experimental methods

### 2.1 Fabrication of metallic porous nanostructures

Porous aluminum oxide structures were fabricated by following a well-established procedure [30]. Briefly, a pure aluminum foil (99.999%, 1 mm thickness) was electropolished in a mixed solution of perchloric acid and ethanol (1/4 vol/vol) with an applied voltage of 20 V (DC) at 7 ℃. The electropolished aluminum foil substrate was rinsed three times with deionized water and dried. The substrate was then anodized in 0.1 M phosphoric acid at 0 ℃ by applying 195 V (DC) for 8 h. The aluminum oxide film formed in the first anodization step was dissolved in a mixed solution of chromic acid (1.8 wt.%) and phosphoric acid (6 wt.%) over 6 h at 65 ℃. After rinsing the substrate with deionized water and ethanol, a second anodization step was performed in the same manner as the first to obtain a hexagonally ordered alumina nanopore structure. The diameter of nanopore was increased at a rate of 0.6 nm/min using 0.1 M phosphoric acid solution at 30 ℃. To obtain the final metallic porous nanostructures, nickel was deposited onto the porous alumina at arate of 4 Å·s$^{-1}$ by vacuum evaporation at 5 × 10$^{-6}$ Torr using an E-beam evaporator [31]. Nickel-based well-ordered metallic porous nanostructures with varying pore sizes formed on the porous alumina structures, which also contained pores of varying size. The surface of the metallic porous nanostructures was examined by scanning electron microscopy (SEM, Hitachi-3400SN) with an accelerating voltage of 10 kV.

### 2.2 Nanoindentation tests

To study the effects of electric potential on the mechanical properties of the metallic porous nanostructures, nanoindentation under an applied potential was performed using a TS 75 TriboScope nanoindentation device (Hysitron, Minneapolis, MN) [32]. A diamond conical indenter tip with a diameter of ~1 μm was used for nanoindentation. An electric circuit was used to apply an electric potential to each nanostructure during nanoindentation. The ammeter was connected with the circuit in series to measure current, while the voltmeter was connected in parallel to measure supply voltage. A tunable DC-mode power source was used to apply a potential to the nanostructures. In order to avoid substrate effects, the total indentation depth did not exceed 20% of the total thickness of the target sample [33].

### 2.3 Methodology of the indentation modulus measurement

To understand the mechanical properties of metallic porous nanostructures, the contact area between two surfaces should be considered when defining the indentation modulus. Various contact models have focused on defining the contact area, including the indention modulus. Since the Hertz contact theory introduced the general contact model for studying mechanical properties [34], a variety of modified contact theories, such as the JKR [35] and DMT [36] theories, have been developed. The indentation modulus can be obtained through indentation experiments [37]. Figure 1 demonstrates a typical load-displacement curve during an indentation experiment. The indentation modulus can be determined from the unloading stiffness. The unloading stiffness is expressed by Eq. (1):

$$\frac{\mathrm{d}P}{\mathrm{d}h}=\frac{2}{\sqrt{\pi}}K\sqrt{A} \tag{1}$$

where $P$ is the applied load, $h$ is the indentation displacement, $K$ is the indentation modulus, and $A$ is the contact area [37]. From Eq. (1), the indentation modulus may be specified by Eq. (2):

$$K=\frac{1}{\beta}\frac{\sqrt{\pi}}{2}\frac{\left(\frac{\mathrm{d}P}{\mathrm{d}h}\right)}{\sqrt{A}} \tag{2}$$

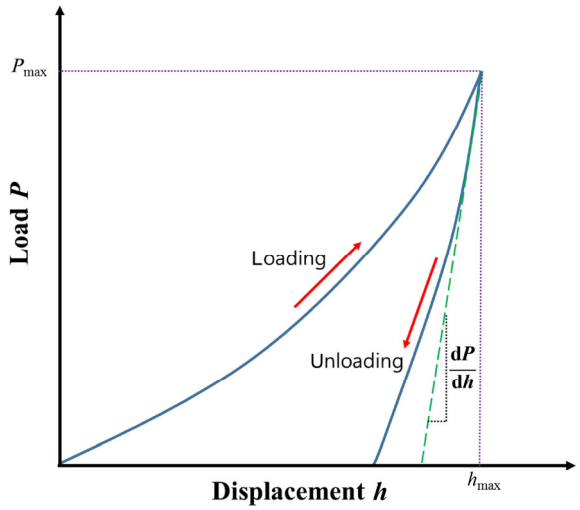


**Fig. 1** Schematic diagram of a typical load displacement curve during an indentation experiment.

where $\beta$ is the conversion factor determined by the type of indenter tip used. For a conical indenter tip, $\beta = 1.08$ [38, 39].

Using the applied load and indentation distance curve measurement function of the nanoindentation, the indentation moduli of the metallic porous nanostructures were measured with an accompanying applied electric potential. Figure 2 shows a SEM image of the conical indenter tip and a schematic of the nanoindentation setup with an applied electric potential. The radius of the conical tip used for these experiments was approximately 500 nm (Figs. 2(a), 2(b), and Fig. S1 in the Electronic Supplementary Material (ESM)), and electric potential was applied to the nanostructure using the circuit configuration shown in Fig. 2(c) (see additional image Fig. S2 in the ESM). The nanoindentation experiment was a load control basis test, and multiple loads from 300 to 900 μN were applied to the nanostructure surface to precisely determine the mechanical properties of the nanostructures with a target indentation depth range of 5 to 50 nm. The indentation modulus of each sample was measured by the Oliver-Pharr method using the obtained load displacement curves [37].

## 3 Results and discussion

### 3.1 Load indentation depth analysis

Figure 3 shows the applied loads and resulting indentation depth curves from metallic porous nanostructures with various pore sizes. In each case, the indentation modulus could be measured by the slope of the unloading curve. Greater stiffness (d$P$/d$h$) on the curve corresponded to a greater indentation modulus. As the Fig. 3 indicates, the slope of the unloading curve decreased as the pore size of the metallic porous nanostructures increased. Moreover, the corresponding indentation depth increased with an increase in pore size. As the indentation modulus is related with mechanical properties of the materials, larger pore size corresponded with degradation of the mechanical properties of the materials [40, 41]. Additionally, increased pore size naturally led to increased porosity of the nanostructures. The results of this experiment demonstrated that the indentation modulus decreased

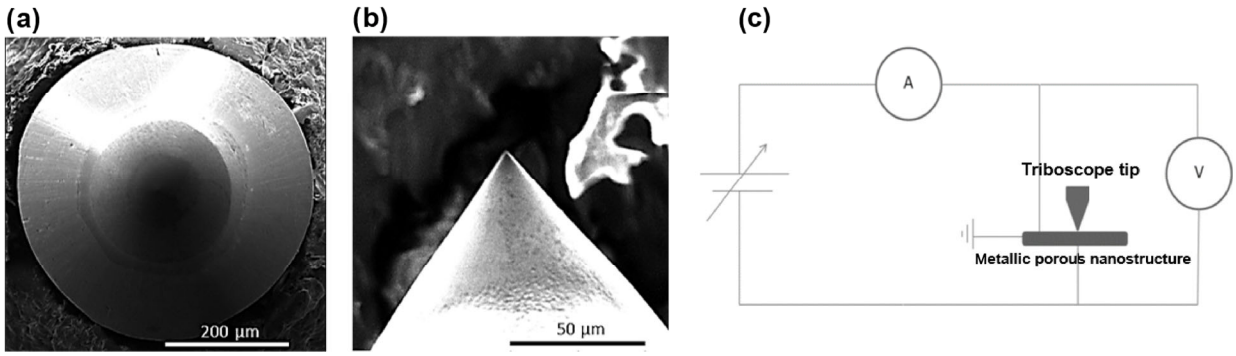


**Fig. 2** SEM images of the conical indenter tip. (a) Top view of the conical tip, (b) side view of the conical tip, and (c) schematic setup for nanoindentation with applied electric potential.

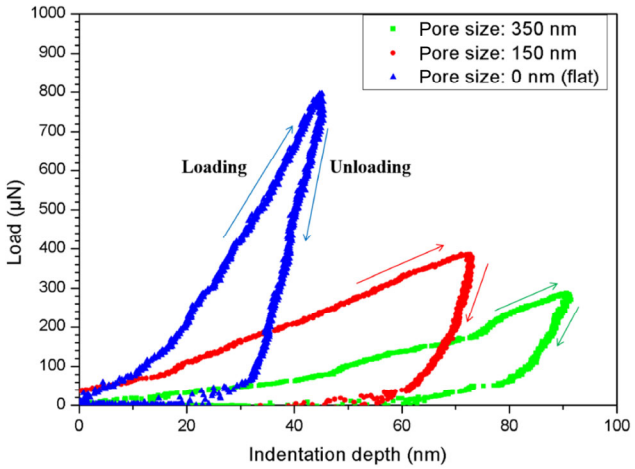


**Fig. 3** Representative load and indentation depth curves for metallic porous nanostructures with various pore sizes.

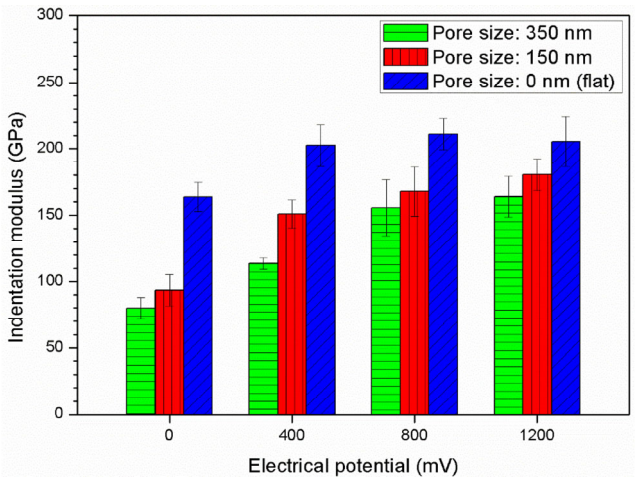


**Fig. 4** Indentation modulus versus applied electric potential in metallic porous nanostructures with various pore sizes.

as the pore size of the metallic porous nanostructures increased.

### 3.2 Electric potential-induced indentation modulus

The effect of electric potential on the indentation modulus was determined when electric potential was applied to the metallic porous nanostructures during the indentation experiments. Figure 4 shows the indentation moduli of nanostructures with various pore sizes according to the applied electric potential. As the Fig. 4 shows, the indentation modulus observed without an applied electric potential (0 mV) decreased as the pore size of metallic porous nanostructures increased. Without application of electric potential, the indentation moduli of flat nanostructures with no pores (pore size = 0 nm) and nanostructures with pore sizes of 150 and 350 nm were 163.8, 93.6, and 79.9 GPa, respectively. These results correlated with the load and indentation depth curve results. Moreover, the indentation moduli showed an overall increasing trend as the applied electric potential increased. Results indicated that the electric potential affected the electronic and atomic structures of nanostructuresurfaces in accordance with the observed indentation modulus behavior [27, 28]. In other words, the increase of the indentation modulus with electric potential can be related to the alteration of atomic scale bond strength of metallic porous nanostructures by applying electric potential [28].

### 3.3 Contact area analysis between the indenter tip and the metallic porous nanostructures

The contact area between two surfaces is a critical factor that influences tribological properties, such as friction behaviors and adhesive properties [41]. It is possible to estimate the radius of contact area '*a*' with

Hertzian contact theory using Eq. (3) [34]:

$$a^3 = \frac{3PR_1}{4K} \tag{3}$$

where $R_1$ is the radius of a conical tip. The Hertzian contact theory is usually used to determine the contact area between a conical-type indenter tip and a flat surface. In order to precisely evaluate the contact area, details of the geometric shape of the substrate contacted with the conical type indenter tip must be systematically analyzed. Figure 5 shows SEM images of a metallic porous nanostructure and schematics for contact area determination (see additional image Fig. S3 in the ESM). The contact area between the conical tip and the metallic porous structures was calculated by deducting the porous area of the nanostructures from the projected contact area between the conical tip and the nanostructures as highlighted in Fig. 5(a). Notably, the shape of the nanostructure was used to determine the actual contact area. As discussed in our previous study, the surfaces of fabricated metallic porous nanostructures on porous alumina had a crown shape, which can be seen in Figs. 5(b) and 5(c) [42]. The crown shape of the nanostructures affected calculation of the contact area. As illustrated in Fig. 5(d), the unit contact model can be used to accurately identify the contact area influenced by the pore structure. Owing to the crown shape of the metallic porous nanostructure, the unit contact model can be employed when the indenter tip approaches the nanostructure. Although the shape of nickel-based metallic porous nanostructures can be deformed by applying external forces, the deformation of the nanostructures under local pressure through the indenter tip can be quite small and is assumed to be negligible.

The equivalent diameter of the porous area ($d_{eq}$) can be determined at the top surfaces of the crowns, as illustrated in Fig. 5(d), by Eq. (4):

$$d_{eq} = \frac{R_1 \cdot s}{R_1 + R_2} \tag{4}$$

where $s$ is the pore-to-pore distance, and $R_2$ is the radius of the crown. $R_2$ can be determined by geometric relation at the crown wall of the nanostructure shown in Fig. 5(d) by Eq. (5):

$$R_2 = \left(\sqrt{\left(\frac{s-d}{2}\right)^2 + t^2}\right) \Big/ \left(2 \cdot \left(\frac{t}{(s-d)/2}\right)\right) \tag{5}$$

where $d$ is the original pore diameter, and $t$ is the height of the crown. By using the calculated $d_{eq}$, the contact area between the conical tip and the nanostructures

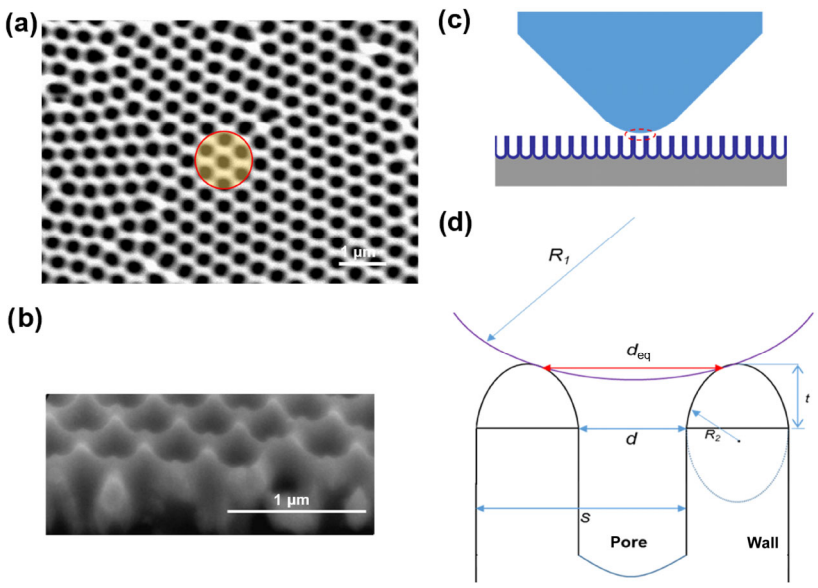


**Fig. 5** Unit contact model of metallic porous nanostructures. (a) SEM top-view image of metallic porous nanostructures with highlighted projected area of the conical tip on the metallic porous nanostructures; (b) SEM tilted-view image of metallic porous nanostructures; (c) schematic illustration of contact between the conical tip and metallic porous nanostructure; (d) detailed illustration of the unit contact model between the conical tip and metallic porous nanostructure.

can be calculated using Eq. (6):

$$\text{Contact area} = \pi a^2 \cdot \left(1 - \frac{-3\pi\left(\frac{d_{eq}}{2}\right)^2}{\frac{3\sqrt{3}}{2}s^2}\right) \quad (6)$$

where $a$ is contact radius determined by Hertz contact theory.

As is known, the contact area can be altered by applying loads of different magnitudes under constant structural conditions. To exclude effects from applied loads during the determination of contact area, the relative values of the contact area were defined as a ratio, which is written as Eq. (7) [41]:

$$\text{Contact area ratio} = \frac{\text{Contact area}_{\text{target}}}{\text{Contact area}_{\text{reference}}} \quad (7)$$

where the reference was configured as a flat surface with no pores (pore size = 0 nm), and the target varied with variations in nanostructure size. By employing the contact area ratio, it was possible to compare relative changes in the contact areas of various nanostructures under applied electric potentials without considering external loading conditions. Figure 6 reveals that pore formation played a key role in contact area determination. Specifically, the contact area ratio decreased when pore size increased. The contact area ratios of nanostructures with no pores (pore size 0 nm) and pore sizes of 150 and 350 nm under 0 mV applied electric potential were 1.00, 0.65, and 0.60, respectively. The contact areas of nanostructures with flat surfaces were larger than those of nanostructures with pore sizes of 150 and 350 nm at all applied electric potentials. This clearly indicated that pore formation caused dramatic increases in the areas deducted from the corresponding projected contact areas, thereby reducing the respective contact areas.

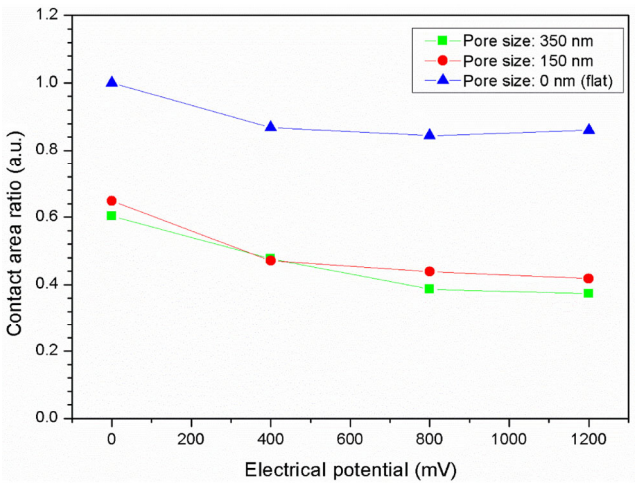


**Fig. 6** Contact area ratio versus applied electric potential from metallic porous nanostructures with various pore sizes.

The decrease in contact area is literally caused by increased pore size. However, the difference between the contact areas of the nanostructures with 150 and 350 nm pores was not significant. This was mainly because the actual deducted area was not determined by pore size but was instead determined by $d_{eq}$. The metallic porous nanostructures with 150 and 350 nm pores had geometrically determined $d_{eq}$ values of 356.6 and 379.1 nm, respectively. Notably, details in the shape of the porous structure were crucial for determining the contact area between solid surfaces. As illustrated in Fig. 7, widening the distance between the etched walls of the porous nanostructure caused an increase in pore size. However, the tops of the crowns were not affected much by the widening process. Thus, $d_{eq}$ in the nanostructure with 350 nm pores did not differ significantly from $d_{eq}$ in the nanostructure with 150 nm pores.

There were small differences between the contact area ratios of the metallic porous nanostructures with 150 and 350 nm pores. As we determined, the indentation modulus was a critical factor in defining the contact area. It is thus worth noting that the indentation modulus was a valid means by which to explain the differences between the contact areas of the nanostructures with 150 and 350 nm pores. The Hertzian contact radius '$a$' decreased with an increase of the indentation modulus. A general trend was thus observed, in which contact area decreased when the indentation modulus increased. The indentation results indicated that the indentation modulus, which can represent the stiffness of the metallic porous nanostructures, increased with increasing applied electric potential. This feature demonstrated that in terms of quantitative analysis, the contact area between the indenter tip and the nanostructures decreased with increased applied electric potential, which is illustrated in Fig. 6. In other words, the contact area decreased with increases in the indentation modulus.

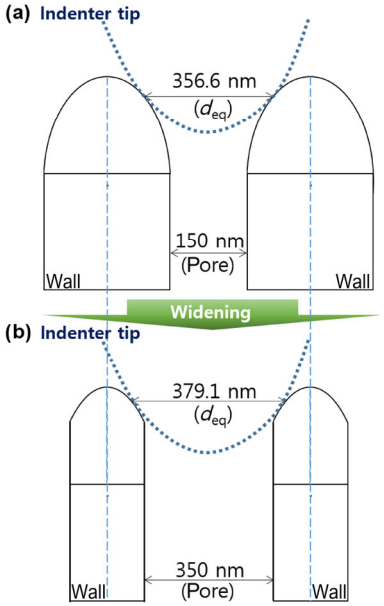


**Fig. 7** Schematic presentation of the equivalent diameter of the porous area ($d_{eq}$). (a) $d_{eq}$ of 150 nm metallic porous nanostructure and (b) $d_{eq}$ of 350 nm metallic porous nanostructure.

The overall behavior in the contact area can explain results of porous nanostructure pull-off force tests. As revealed in previous studies, the pull-off forces, which are influenced by the contact area at the interface, are rarely affected by differences among the pore sizes of porous nanostructures [20, 41]. The source of these pull-off force behaviors becomes obvious once it is clear that the contact area between the solid tip and porous structures depends on the $d_{eq}$, not on pore size. We concluded the geometric shape of a porous structure is a critical factor for determining both its mechanical and tribological properties.

## 4 Conclusions

Effects of an applied electric potential on the surface structure and mechanical properties were investigated in this study. Nickel-based metallic porous nanostructures were fabricated and characterized with nanoindentation. Indentation moduli and contact areas between the conical-type indenter tip and the nanostructures were evaluated by applying electric potential. Results showed that the metallic porous nanostructures stiffened with increases in electric potential. The indentation modulus was dependent not only on pore size, but also on the amount of electric potential applied. The contact area was altered by pore size and the indentation modulus. Furthermore, the contact areas between the indenter tip and the nanostructures were influenced by morphological shape details on the surfaces of the nanostructures. The nickel-based metallic porous nanostructures enabled control of the indentation modulus and contact area through manipulation of electronic and atomic structures by application of electric potential. This property can be used to build mechanically durable and reliable metallic porous nanostructures. Therefore, in terms of robustness, our findings present the possibility of designing various metallic porous nanostructure-based functional devices by employing electric potential and morphological shape differences. In addition, the findings of this study would be useful for expending the scope of future studies of the theoretical examination with respect to electric-mechanical behavior of metallic porous nanostructures.

## Acknowledgements

This work was supported by the National Research Foundation of Korea (NRF) grant funded by the Korea government (MSIT) (No. NRF-2018R1C1B6002339) and by the Chung-Ang University Research Grants in 2017.

**Electronic Supplementary Material**: Supplementary material is available in the online version of this article at https://doi.org/10.1007/s40544-019-0307-1.

## References


[1] Linic S, Christopher P, Ingram D B. Plasmonic-metal nanostructures for efficient conversion of solar to chemical energy. *Nat Mater* **10**(12): 911–921 (2003)

[2] Pilo-Pais M, Watson A, Demers S, LaBean T H, Finkelstein G. Surface-enhanced Raman scattering plasmonic enhancement using DNA origami-based complex metallic nanostructures. *Nano Lett* **14**(4): 2099–2104 (2014)

[3] Chirumamilla M, Toma A, Gopalakrishnan A, Das G, Zaccaria R P, Krahne R, Rondanina E, Leoncini M, Liberale C, De Angelis F. 3D nanostar dimers with a sub-10-nm gap for single-/few-molecule surface-enhanced Raman scattering. *Adv Mater* **26**(15): 2353–2358 (2014)

[4] Zhang S M, Zhang P P, Wang Y, Ma Y Y, Zhong J, Sun X H. Facile fabrication of a well-ordered porous Cu-doped $SnO_2$ thin film for $H_2S$ sensing. *ACS Appl Mater Interfaces* **6**(17): 14975–14980 (2014)

[5] Variola F, Vetrone F, Richert L, Jedrzejowski P, Yi J H, Zalzal S, Clair S, Sarkissian A, Perepichka D F, Wuest J D, et al. Improving biocompatibility of implantable metals by nanoscale modification of surfaces: An overview of strategies, fabrication methods, and challenges. *Small* **5**(9): 996–1006 (2009)

[6] Seung W, Gupta M K, Lee K Y, Shin K S, Lee J H, Kim T Y, Kim S, Lin J J, Kim J H, Kim S W. Nanopatterned textile-based wearable triboelectric nanogenerator. *ACS Nano* **9**(4): 3501–3509 (2015)

[7] Park S J, Seol M L, Kim D, Jeon S B, Choi Y K. Triboelectric nanogenerator with nanostructured metal surface using water-assisted oxidation. *Nano Energy* **21**: 258–264 (2016)

[8] Park C, Song G, Cho S M, Chung J, Lee Y, Kim E H, Kim M, Lee S, Huh J, Park C. Supramolecular-assembled Nanoporous film with switchable metal salts for a triboelectric Nanogenerator. *Adv Funct Mater* **27**(27): 1701367 (2017)

[9] Zeng W, Shu L, Li Q, Chen S, Wang F, Tao X M. Fiber-based wearable electronics: A review of materials, fabrication, devices, and applications. *Adv Mater* **26**(31): 5310–5336 (2014)

[10] Kim S, Zhou Y, Cirillo J D, Polycarpou A A, Liang H. Bacteria repelling on highly-ordered alumina-nanopore structures. *J Appl Phys* **117**(15): 155302 (2015)

[11] Kim S, Polycarpou A A, Liang H. Enhanced-ion transfer via metallic-nanopore electrodes. *J Electrochem Soc* **161**(10): A1475–A1479 (2014)

[12] Zhu C Z, Du D, Eychmüller A, Lin Y H. Engineering ordered and nonordered porous noble metal nanostructures: synthesis, assembly, and their applications in electrochemistry. *Chem Rev* **115**(16): 8896–8943 (2015)

[13] Dong S M, Chen X, Gu L, Zhou X H, Xu H X, Wang H B, Liu Z H, Han P X, Yao J H, Wang L, et al. Facile preparation of mesoporous titanium nitride microspheres for electrochemical energy storage. *ACS Appl Mater Interfaces* **3**(1): 93–98 (2011)

[14] Gao S Y, Jia X X, Yang J M, Wei X J. Hierarchically micro/nanostructured porous metallic copper: Convenient growth and superhydrophilic and catalytic performance. *J Mater Chem* **22**(40): 21733–21739 (2012)

[15] Kim S, Polycarpou A A, Liang H. Electrical-potential induced surface wettability of porous metallic nanostructures. *Appl Surf Sci* **351**: 460–465 (2015)

[16] Zheng J Y, Lv Y H, Xu S S, Han X, Zhang S T, Hao J Y, Liu W M. Nanostructured TiN-based thin films by a novel and facile synthetic route. *Mater Des* **113**: 142–148 (2017)

[17] Xu Y, Zhang B. Recent advances in porous Pt-based nanostructures: Synthesis and electrochemical applications. *Chem Soc Rev* **43**(8): 2439–2450 (2014)

[18] Velev O D, Tessier P M, Lenhoff A M, Kaler E W. Materials: A class of porous metallic nanostructures. *Nature* **401**(6753): 548 (1999)

[19] Lee W, Park S J. Porous anodic aluminum oxide: anodization and templated synthesis of functional nanostructures. *Chem Rev* **114**(15): 7487–7556 (2014)

[20] Kim S, Polycarpou A A, Liang H. Active control of surface forces via nanopore structures. *APL Mater* **1**(3): 032118 (2013)

[21] Zhu C, Wen D, Oschatz M, Holzschuh M, Liu W, Herrmann A K, Simon F, Kaskel S, Eychmüller A. Kinetically controlled synthesis of PdNi bimetallic porous nanostructures with enhanced electrocatalytic activity. *Small* **11**(12): 1430–1434 (2015)

[22] Sk M, Yue C Y, Ghosh K, Jena R K. Review on advances in porous nanostructured nickel oxides and their composite electrodes for high-performance supercapacitors. *J Power Sources* **308**: 121–140 (2016)

[23] Duan J J, Chen S, Zhao C. Strained nickel phosphide nanosheet array. *ACS Appl Mater Interfaces* **10**(36): 30029–30034 (2018)

[24] Niu X H, Lan M B, Zhao H L, Chen C. Highly sensitive and selective nonenzymatic detection of glucose using three-dimensional porous nickel nanostructures. *Anal Chem* **85**(7): 3561–3569 (2013)

[25] Zhang L, Jin L, Zhang B B, Deng W L, Pan H, Tang J F, Zhu M H, Yang W Q. Multifunctional triboelectric nanogenerator based on porous micro-nickel foam to harvest mechanical energy. *Nano Energy* **16**: 516–523 (2015)

[26] Yue Y, Juarez-Robles D, Chen Y, Ma L, Kuo W C H, Mukherjee P, Liang H. Hierarchical structured Cu/Ni/$TiO_2$ nanocomposites as electrodes for lithium-ion batteries. *ACS Appl Mater Interfaces* **9**(34): 28695–28703 (2017)

[27] Klimov N N, Jung S, Zhu S Z, Li T, Wright C A, Solares S D, Newell D B, Zhitenev N B, Stroscio J A. Electromechanical properties of graphene drumheads. *Science* **336**(6088): 1557–1561 (2012)

[28] Chien T, Liu J, Yost A J, Chakhalian J, Freeland J W, Guisinger N P. Built-in electric field induced mechanical property change at the lanthanum nickelate/Nb-doped strontium titanate interfaces. *Sci Rep* **6**: 19017 (2016)

[29] Kim M S, Vinh N T, Yu H H, Hong S T, Lee H W, Kim M J, Han H N, Roth J T. Effect of electric current density on the mechanical property of advanced high strength steels under quasi-static tensile loads. *Int J Prec Eng Manuf* **15**(6): 1207–1213 (2014)
[30] Masuda H, Fukuda K. Ordered metal nanohole arrays made by a two-step replication of honeycomb structures of anodic alumina. *Science* **268**(5216): 1466–1468 (1995)
[31] Kim S, Lee S, Choi D, Lee K, Park H, Hwang W. Fabrication of metal nanohoneycomb structures and their tribological behavior. *Adv Compos Mater* **17**(2): 101–110 (2008)
[32] Yu N, Polycarpou A A, Conry T F. Tip-radius effect in finite element modeling of sub-50 nm shallow nanoindentation. *Thin Solid Films* **450**(2): 295–303 (2004)
[33] Tayebi N, Polycarpou A A, Conry T F. Effects of substrate on determination of hardness of thin films by nanoscratch and nanoindentation techniques. *J Mater Res* **19**(6): 1791–1802 (2004)
[34] Hertz H R. *Uber die Beruhrung fester elastischer Korper und Uber die Harte*. Berlin: Verhandlung des Vereins zur Beforderung des GewerbefleiBes, 1882: 449.
[35] Johnson K L, Kendall K, Roberts A D. Surface energy and the contact of elastic solids. *Proc Roy Soc A* **324**(1558): 301–313 (1971)
[36] Derjaguin B V, Muller V M, Toporov Y P. Effect of contact deformations on the adhesion of particles. *J Colloid Interface Sci* **53**(2): 314–326 (1975)
[37] Oliver W C, Pharr G M. An improved technique for determining hardness and elastic modulus using load and displacement sensing indentation experiments. *J Mater Res* **7**(6): 1564–1583 (1992)
[38] Hay J C, Bolshakov A, Pharr G M. A critical examination of the fundamental relations used in the analysis of nanoindentation data. *J Mater Res* **14**(6): 2296–2305 (1999)
[39] Johnson K L. *Contact Mechanics*. Cambridge (USA): Cambridge University Press, 1987.
[40] Ishizaki K, Komarneni S, Nanko M. *Porous Materials*: *Process Technology and Applications*. Boston (USA): Springer, 1998.
[41] Choi D, Lee S, Kim S, Lee P, Lee K, Park H, Hwang W. Dependence of adhesion and friction on porosity in porous anodic alumina films. *Scr Mater* **58**(10): 870–873 (2008)
[42] Kim S, Choi H, Polycarpou A A, Liang H. Morphology-influenced wetting model of nanopore structures. *Friction* **4**(3): 249–256 (2016)

**Sunghan KIM.** He is an assistant professor of School of Mechanical Engineering at Chung-Ang University. He received his Ph.D. degree in J. Mike Walker ’66 Department of Mechanical Engineering at Texas A&M University in 2015. His research interests lie in establishing essential design factors to optimize the tribological and mechanical properties of sustainable functional nanocomposites for biological, electrochemical, and mechanical applications.

**Andreas A. POLYCARPOU**. He is James J. Cain Chair and Meinhard H. Kotzebue’14 professor and department head of J. Mike Walker ’66 Department of Mechanical Engineering at Texas A&M University. His tribological research has been primarily focused on contact mechanics related to miniature systems. Recent emphasis has been on the tribology of devices for reduced energy and improved environmental-related impact, such as the use of carbon dioxide as a natural refrigerant and the use of surface treatments towards oil-lees machine operation.

**Hong LIANG**. She is Oscar S. Wyatt Jr. professor at J. Mike Walker ’66 Department of Mechanical Engineering, Texas A&M University. Her research interests have been in fundamental aspects of friction, wear, and lubrication. Her group carries out research in design and synthesis of advanced materials that have unique characteristics to be applied for tribological applications including lubrication, wear protection, and chemical-mechanical polishing. The group develops alternative approaches to probe material surfaces during tribological process.